Luminescence and Single-Molecule-Magnet Behaviour in Lanthanide Coordination Complexes Involving Benzothiazole-Based Tetrathiafulvalene Ligands

Y. Kishi, L. Cornet, Fabrice Pointillart, François Riobé, B. Lefeuvre, O. Cador, Boris Le Guennic, O. Maury, H. Fujiwara, L. Ouahab

Luminescence and Single-Molecule Magnet Behaviour in Lanthanide Coordination Complexes Involving Benzothiazole-Based Tetrathiafulvalene Ligands

Y. Kishi,[a],[b] L. Cornet,[a] F. Pointillart,*[a] F. Riobé,[c] B. Lefeuvre,[a] O. Cador,[a] B. Le Guennic,[a] O. Maury,[c] H. Fujiwara,*[b] L. Ouahab[a]

Keywords: Tetrathiafulvalene / Lanthanides / Coordination Chemistry / Luminescence / Single-Molecule Magnet

The two 4-[6-(1,3-benzothiazol-2-yl)pyridin-3-yl]-4',5'-bis(methylthio)tetrathiafulvene (**L^1**) and 4-[6-(1,3-benzothiazol-2-yl)pyridin-3-yl]-4',5'-(ethylenedithio)tetrathiafulvene (**L^2**) ligands have been elaborated and six new coordination complexes of lanthanide ions, namely $[Ln_2(hfac)_6(\mathbf{L^1})_2]\cdot C_6H_{14}\cdot xCH_2Cl_2$ (Ln = Dy and x = 0.25 (**1**); Ln = Yb and x = 0.30 (**2**)), $[Ln(hfac)_3(\mathbf{L^2})]$ (Ln = Dy (**3**), Yb (**4**)) and $[Ln(tta)_3(\mathbf{L^1})]$ (Ln = Yb (**5**), Er (**6**)) ($hfac^-$ = 1,1,1,5,5,5-hexafluoroacetylacetonate; tta^- = 2-thenoyltrifluoroacetylacetonate), have been characterized by X-ray diffraction on single crystals. Compounds **1**-**6** have been identified as mononuclear complexes with different crystal packing depending on the nature of the ancillary and tetrathiafulvalene-based ligands. The two dysprosium derivatives **1** and **3** displayed Single-Molecule Magnet behaviour in zero-applied magnetic field. While the near-infrared luminescence of **2** and **4** is almost undetectable, the change of ancillary ligands switched on the Yb^{III} (**5**) and Er^{III} (**6**) luminescence.

[a] Institut des Sciences Chimiques de Rennes, UMR 6226 CNRS-Université de Rennes 1, 263 Avenue du Général Leclerc 35042 Rennes Cedex, France.
Tel : +33223236752
E-mail: fabrice.pointillart@univ-rennes1.fr
http://www.scienceschimiques.univ-rennes1.fr
[b] Department of Chemistry, Graduate School of Science, Osaka Prefecture University, 1-1 Gakuen-cho, Naka-ku, Sakai, Osaka, 599-8531, Japan.
[c] Laboratoire de Chimie, UMR 5182 CNRS-ENS Lyon-Université Lyon 1, 46 Allée d'Italie, 69364 Lyon Cedex

Supporting information for this article is available on the WWW under http://www.eurjic.org/ or from the author.

Introduction

Lanthanide ions are very fascinating elements intensively used in the design of Single-Molecule Magnets (SMMs)[1]-[4] and luminescent molecular materials[5]-[7]. The origin of this keen interest comes from their particular magnetic characteristic (high magnetic moment and strong magnetic anisotropy) and specific luminescence. Both SMMs and luminescent materials have respectively plethora of potential applications for high-density data storage, spintronics and quantum computing,[8]-[15] OLEDs,[16] time-resolved fluoro-immunoassays[17], biosensors[18][19] and time-resolved imaging[20]. It is worth to notice that in the molecular magnetism field, the luminescence was recently exploited to reach a high level of comprehension of the magnetic properties.[21]-[29] Obviously the coexistence of both magnetic and optical properties participates to enrich the family of multi-properties magnetic objects with the emergence of luminescent SMMs. A certain number of prerequisites are needed to favour both the observation of SMM behaviour and lanthanide luminescence. The strategy of our group is to use tetrathiafulvalene-based ligands as structural agents and organic chromophores in order to magnetically separate the spin carriers and sensitize the luminescence through an antenna effect. In the best cases, redox-active luminescent SMMs have been designed.[23][30] Historically, TTF derivatives have been used for their donating abilities leading to potential electronic conductivity.[31] It has been demonstrated that a fruitful strategy is to add to the TTF core localized electrons thanks to transition metals (3*d* and 4*d*)[32]-[37] or lanthanides[30][38]. Such π-*d* and π-*f* systems have shown exciting transport properties such as antiferromagnetic-superconductor or magnetic-field induced superconducting transition[39]-[40]. To design the previously mentioned π-*d* and π-*f* systems, the TTF core must be decorated with an accepting group able to coordinate the metal center. The latter group can be active in the observation of conducting properties.

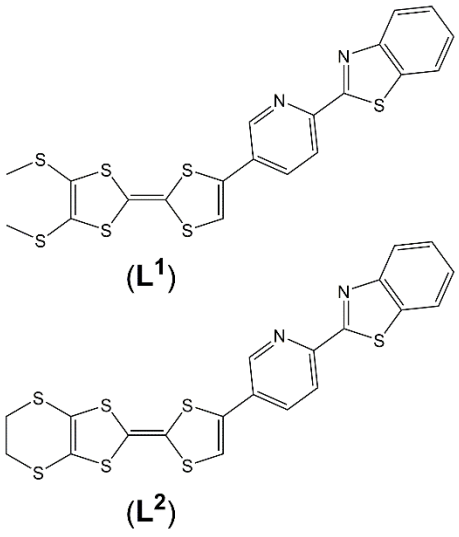

Scheme 1. Molecular structure of **L^1** and **L^2**.

Table 1. X-ray crystallographic data for the complexes **1**-**6**.

Compounds	$[Dy_2(hfac)_6(\mathbf{L^1})_2]\cdot C_6H_{14}\cdot 0.25CH_2Cl_2$ (**1**)	$[Yb_2(hfac)_6(\mathbf{L^1})_2]\cdot C_6H_{14}\cdot 0.3CH_2Cl_2$ (**2**)	$[Dy(hfac)_3(\mathbf{L^2})]$ **(3)**
Formula	$C_{76.5}H_{48.5}Cl_{0.5}Dy_2F_{36}N_4O_{12}S_{14}$	$C_{76.3}H_{48.6}Cl_{0.6}Yb_2F_{36}N_4O_{12}S_{14}$	$C_{35}H_{15}DyF_{18}N_2O_6S_7$
M / g.mol^{-1}	2688.25	2713.6	1288.41
Crystal system	Triclinic	Triclinic	Monoclinic
Space group	P-1 (N°2)	P-1 (N°2)	C2/c (N°15)
Cell parameters	a = 15.0946(12) Å	a = 15.0778(7) Å	a = 29.536(10) Å
	b = 16.4740(12) Å	b = 16.5194(8) Å	b = 22.365(9) Å
	c = 22.1007(17) Å	c = 22.0501(9) Å	c = 16.845(6) Å
	α = 73.488(3)°	α = 73.266(2)°	
	β = 72.917(4)°	β = 72.757(2)°	β = 91.32(2)°
	γ = 79.242(4)°	γ = 79.066(2)°	
Volume / Å^3	5004.6(7)	4990.4(4)	11124(7)
Cell formula units	2	2	8
T / K	150 (2)	150(2)	150(2)
Diffraction reflection	$1.99 \leq 2\theta \leq 54.90$	$2.00 \leq 2\theta \leq 55.05$	$2.28 \leq 2\theta \leq 55.20$
ρ_{calc}, g.cm^{-3}	1.784	1.806	1.539
μ, mm^{-1}	1.911	2.296	1.704
Number of reflections	67664	65829	38466
Independent reflections	21485	22733	12720
$Fo^2 > 2\sigma(Fo)^2$	12678	15838	4357
Number of variables	1282	1270	598
R_{int}, R_1, wR_2	0.0697, 0.0695, 0.1840	0.0500, 0.0543, 0.1528	0.1035, 0.0783, 0.2117
Compounds	$[Yb(hfac)_3(\mathbf{L^2})]$ **(4)**	$[Yb(tta)_3(\mathbf{L^1})]$ **(5)**	$[Er(tta)_3(\mathbf{L^1})]$ **(6)**
Formula	$C_{35}H_{15}DyF_{18}N_2O_6S_7$	$C_{44}H_{26}YbF_9N_2O_6S_{10}$	$C_{44}H_{26}ErF_9N_2O_6S_{10}$
M / g.mol^{-1}	1299.0	1343.3	1337.5
Crystal system	Monoclinic	Monoclinic	Monoclinic
Space group	C2/c (N°15)	$P2_1/a$ (N°14)	$P2_1/a$ (N°14)
Cell parameters	a = 29.320(7) Å	a = 11.8783(19) Å	a = 11.8689(7) Å
	b = 22.452(5) Å	b = 26.127(5) Å	b = 26.1037(17) Å
	c = 16.786(3) Å	c = 18.337(3) Å	c = 18.4693(13) Å
	β = 91.727(8)°	β = 93.405(7)°	β = 93.565(3)°
Volume / Å^3	11045(4)	5680.7(17)	5711.1(6)
Cell formula units	8	4	4
T / K	150 (2)	150(2)	150(2)
Diffraction reflection	$2.28 \leq 2\theta \leq 55.10$	$6.00 \leq 2\theta \leq 54.97$	$2.21 \leq 2\theta \leq 55.28$
ρ_{calc}, g.cm^{-3}	1.562	1.571	1.556
μ, mm^{-1}	2.057	2.087	1.908
Number of reflections	37248	89275	47161
Independent reflections	12625	16974	13022
$Fo^2 > 2\sigma(Fo)^2$	4333	10732	6672
Number of variables	616	613	643
R_{int}, R_1, wR_2	0.1150, 0.0806, 0.2188	0.1408, 0.0874, 0.1861	0.0845, 0.0698, 0.1830

For example, photo-switchable conductors and photoelectric conversion materials were achieved by synthesizing the TTF-CH=CH-BZT (BZT=1,3-benzothiazole) ligand.[41] In these systems, a charge-separated state is observed for TTF-CH=CH-BZT thank to a photo-induced intramolecular electron transfer giving rise to the generation of photocurrent along the segregated stacks of TTF and BZT moieties. Recently, coordination complexes involving neutral and radical cation forms of this ligand were obtained by some of us.[42] The 4-[6-(1,3-benzothiazol-2-yl)pyridin-3-yl]-4',5'-bis(methylthio)tetrathiafulvene ligand (**L^1**) (Scheme 1) was used to elaborate mononuclear SMMs and study the isotopic effect on the slow magnetic relaxation for two polymorphs.[43]

In the present paper, the influence of the ancillary ligand ($hfac^-$ = 1,1,1,5,5,5-hexafluoroacetyacetonate and tta^- = 2-thenoyltrifluoroacetonate) as well as the nature of the donating core (BMT-TTF = bis(methylthio)tetrathiafulvalene for **L^1** and EDT-TTF = (ethylenedithio)tetrathiafulvalene for **L^2**) on both emissive and magnetic properties was studied.

Results and Discussion

Crystal structure analysis

$[Ln_2(hfac)_6(L^1)_2]\cdot C_6H_{14}\cdot xCH_2Cl_2$ (Ln = Dy and x = 0.25 (1); Ln = Yb and x = 0.30 (2)). Compounds **1** and **2** are isostructural, then only the X-ray structure of **1** is described in details while the values for **2** are given in brackets. **1** and **2** crystallized in the triclinic space group P-1 (N°2) (Table 1). The asymmetric unit (Figures 1, S1 and S2) is composed of two molecules of $[Ln(hfac)_3(\mathbf{L^1})]$, one *n*-hexane molecule and a quarter of dichloromethane molecule of crystallization. The lanthanide ions are surrounded by two nitrogen atoms coming from the bischelating **L^1** ligand and six oxygen atoms coming from the three $hfac^-$ ancillary ligand. The arrangement of the first neighbouring atoms (Table S1) leads to strongly distorted square antiprism (D_{4d} symmetry) coordination polyhedron. The distortion is visualized by continuous shape measurements performed with

SHAPE 2.1 (Table S2).[44] It is worth to note that the distortion is more pronounced for the Dy2 polyhedron ($CShM_{SAPR-8}$=1.145) than for the Dy1 one ($CShM_{SAPR-8}$=0.626) (Table S2).

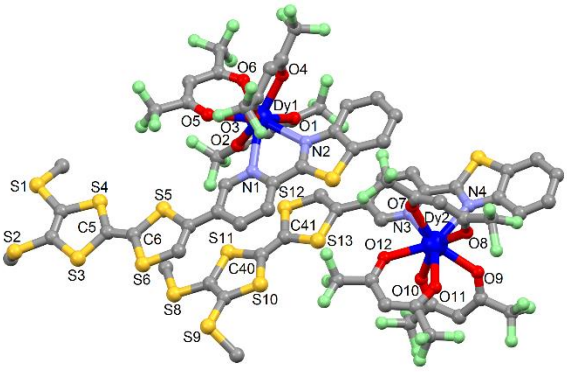

Figure 1. Asymmetric unit of the molecular structure of **1**. Hydrogen atoms and solvent molecules of crystallization are omitted for clarity.

The C=C central bond lengths of 1.336 Å and 1.337 Å [1.315 Å and 1.351 Å] attest to the neutrality of the $\mathbf{L^1}$ ligands in **1** and **2**.
The crystal packing revealed the formation of two columns of stacked ligands. Donor (TTF)-Acceptor (BZT) interactions are found in the column along the *b* axis while D-D interactions are identified between the columns through lateral short contacts S2···S8 = 3.585 Å [3.597 Å] (Figure 2). The shortest intermolecular Dy···Dy distance is equal to 8.795 Å [8.817 Å].

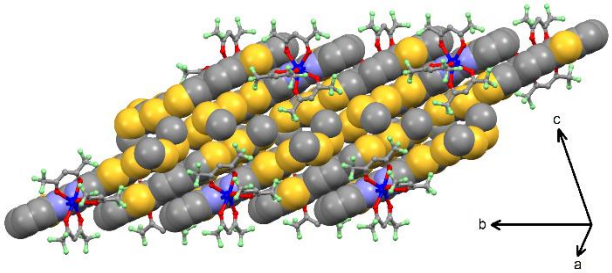

Figure 2. Crystal packing of **1**. The donor part (BMT-TTF core) and the acceptor parts (pyridine and 1,3-benzothiazole groups) are shown in spacefill representation while the $hfac^-$ ligands are shown in ball and sticks representation.

$[Ln(hfac)_3(L^2)]$ (Ln = Dy (3) and Yb (4)). Compounds **3** and **4** are isostructural, then only the X-ray structure of **3** is described in details while the values for **4** are given in brackets. The donor part (EDT-TTF core) and the acceptor parts (pyridine and 1,3-benzothiazole groups) are shown in spacefill representation while the $hfac^-$ ligands are shown in ball and sticks representation. The two compounds crystallized in the monoclinic space group C2/c (N°15) (Table 1). The asymmetric unit is composed of one molecule of $[Ln(hfac)_3(\mathbf{L^2})]$ (Figures 3 and S3). Similarly to the mononuclear complexes involving $\mathbf{L^1}$, the lanthanide ions are coordinated to two nitrogen atoms and six oxygen atoms coming from the $\mathbf{L^2}$ ligands and the three $hfac^-$ anions, respectively. The arrangement of the first neighbouring atoms (Table S3) leads to a slightly distorted square antiprism (D_{4d} symmetry, $CShM_{SAPR-8}$=0.300)[44] coordination polyhedron (Table S2). The C=C central bond lengths of 1.315 Å [1.376 Å] attest to the neutrality of the $\mathbf{L^2}$ ligands in **3** and **4**.

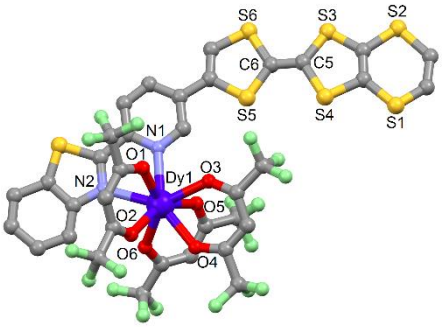

Figure 3. Asymmetric unit of the molecular structure of **3**. Hydrogen atoms are omitted for clarity.

The crystal packing of **3** and **4** is very similar to the one for and **2** (Figure 4). The lateral short contacts S2···S2 is equal to 3.23 Å [3.214 Å] and the shortest intermolecular Dy···Dy [Yb···Yb distance is equal to 8.455 Å [8.426 Å]. Few years ago, some of u demonstrated that slight chemical changes on the TTF core could lea to different crystal packing, modification of the coordination spher symmetry and drastic switch of the magnetic properties.[45] With **L** and $\mathbf{L^2}$, the crystal packing remains almost unchanged and only sligh symmetrisation of the coordination sphere occurred.

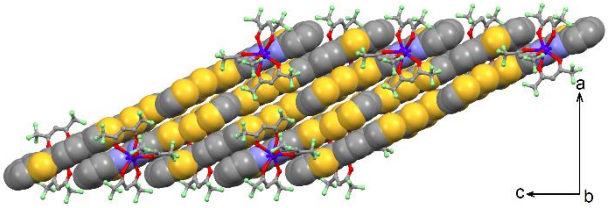

Figure 4. Crystal packing of **3**. The donor part (EDT-TTF core) and th acceptor parts (pyridine and 1,3-benzothiazole groups) are shown in spacefi representation while the $hfac^-$ ligands are shown in ball and stick representation.

$[Ln(tta)_3(L^1)]$ (Ln = Yb (5) and Er (6)). **5** and **6** are isostructural an **6** is taken as representative example. They crystallized in th monoclinic space group $P2_1/n$ (N°14) (Table 1). The asymmetric un is composed of one molecule of $[Ln(tta)_3(\mathbf{L^1})]$. The $Ln(tta)_3$ metal precursor is coordinated to the nitrogenated bischelating coordinatio site of the benzothiazole-2-pyridine moiety. The Ln^{III} ion is in a N_2C square antiprism environment (D_{4d} symmetry) (Table S3) made of si oxygen and two nitrogen atoms that belong to three tta^- anions an one $\mathbf{L^1}$ ligand, respectively (Figures 5).

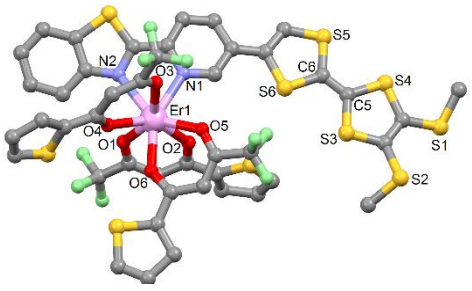

Figure 5. Asymmetric unit of the molecular structure of **6**. Hydrogen atoms are omitted for clarity.

The respective ORTEP views for the complexes **5** and **6** are depicted in Figures S5 and S6. It was previously demonstrated that the rotation of the ligand $\mathbf{L^1}$ happens depending on the size of the lanthanide ion.[43] The isomer observed in **5** and **6** is in agreement with the monoclinic phase observed for the Y^{III} and Dy^{III} analogues. Here again, the C=C central bond length of the TTF core attests to the neutrality of $\mathbf{L^1}$ (C5=C6=1.332(14) Å) [C5=C6=1.312(19) Å].

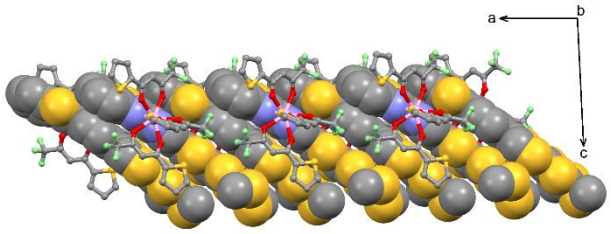

Figure 6. Crystal packing of **5**. The donor part (BMT-TTF core) and the acceptor parts (pyridine and 1,3-benzothiazole groups) are shown in spacefill representation while the tta^- ligands are shown in ball and sticks representation.

The crystal packing of **5** shows that the ligands are packed along the a axis through the S2···S5=3.777 Å [3.838 Å] contacts while the 1D organic networks interact through S···S contacts between the thiomethyl groups and the thiophene rings of tta^- anions.

Electrochemical Properties

The redox properties of $\mathbf{L^1}$ and $\mathbf{L^2}$ and the related complexes are investigated by cyclic voltammetry (Figure S7) and the values of the oxidation potentials are listed in Table S4. The cyclic voltamograms for $\mathbf{L^1}$ ($\mathbf{L^2}$) show two mono-electronic oxidations at 0.51 V and 0.93 V (0.52 V and 0.93 V) corresponding to the formation of a radical cation and a dication of the TTF fragment, respectively (Figure S7). Upon coordination of the lanthanide, the electrochemistry highlights slight anodic shift of the oxidation potentials (average values of 0.53 V and 0.95 V) due to the electron attracting $Ln(hfac)_3$/$Ln(tta)_3$ fragments (Table S4). This subtle effect will be more deeply studied with the absorption spectroscopy (*vide infra*). The reversibility of the oxidation potentials is conserved and the electrochemical properties attest to the redox-activity of $\mathbf{L^1}$ and $\mathbf{L^2}$ in the complexes.

Photophysical Properties

Absorption Properties

The UV-visible absorption properties of $\mathbf{L^1}$ and its $Y^{III}(tta)_3$ analogue[43] have been studied in a CH_2Cl_2 solution (Figures 7a and 7c). Rationalization by TD-DFT calculations was performed following a computational strategy already used successfully on TTF-based systems (see Computational details) (Figures 7b and 7d).[46],[47] The molecular orbital diagrams are depicted on Figure 8. The experimental absorption curve of $\mathbf{L^1}$ has been decomposed into six bands (Figure 7a and Table 2). The calculated UV-visible absorption spectrum for $\mathbf{L^1}$ well reproduces the experimental curve (Figures 7a and 7b). The lowest energy band (22000 cm^{-1}, red Gaussian decomposition) was attributed to π-π* HOMO → LUMO TTF to benzothiazole-2-pyridine charge transfers (ILCT) (Figure 7a, Table 2). All other absorption bands were attributed to ILCT or Intra-TTF (ID) transitions. The UV-visible absorption properties of Y^{III} analogue have been also studied in a CH_2Cl_2 solution (Figure 7c) and rationalized by TD-DFT calculations in order to determine the effect of the metal coordination.

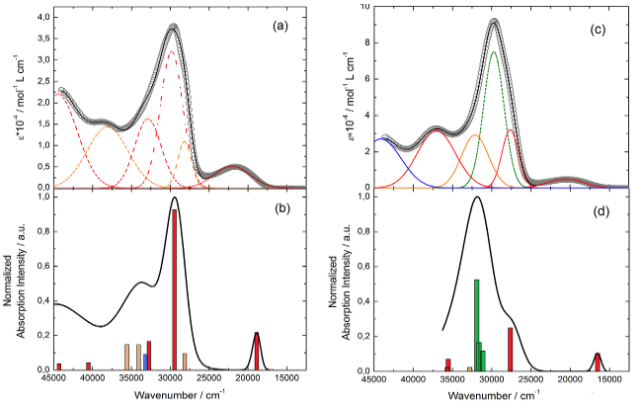

Figure 7. Experimental UV-visible absorption spectrum of $\mathbf{L^1}$ (a) and it $Y(tta)_3$ analogue (c) in CH_2Cl_2 solution (C=4×10^{-5} mol.L^{-1}) (open grey circles Respective Gaussian decompositions (dashed lines) and best fit (full blac line) (R=0.9986 for $\mathbf{L^1}$ and R=0.9997 for the $Y(tta)_3$ analogue). Theoretic absorption spectra of $\mathbf{L^1}$ (b) and its $Y(tta)_3$ analogue (d) (black line). The stick represent the mean contributions of the absorption spectra.

The experimental absorption curve of the $Y(tta)_3$ analogue ha been decomposed into six bands (Figure 7c and Table 2). Th calculated UV-visible absorption spectrum well reproduces th experimental curve (Figures 7c and 7d). The lowest energy ban (20500 cm^{-1}, red Gaussian decomposition) was attributed to π-π HOMO → LUMO TTF to benzothiazole-2-pyridine charge transfer (ILCT) as for the free ligand. The complexation induces a red shift c the ligand-centred ILCT transition due to the Lewis acid behaviour c the $Y(tta)_3$ moiety enforcing the electron withdrawing character of th benzothiazole-2-pyridine fragment. Thus, the absorption bands ar red-shifted to 1500 cm^{-1} (calculated 2352 cm^{-1}) in coordinatio complexes compared to those in $\mathbf{L^1}$. Since the shift value i determined from the data in CH_2Cl_2 solution, this is a first indicatio of the stability of the complexes in such solvent.

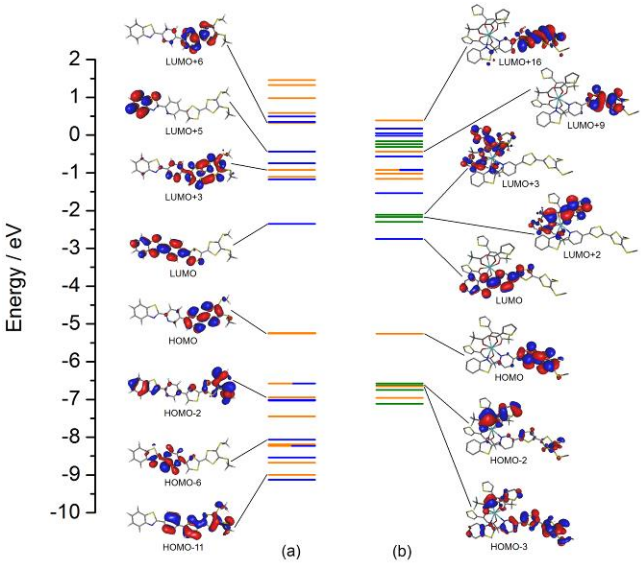

Figure 8. Molecular orbital diagram of $\mathbf{L^1}$ (a) and its $Y(tta)_3$ derivative (b). The energy levels of the centred TTF, benzothiazole-2-pyridine and 2-thenoyltrifluoroacetonate orbitals are represented in orange, blue and green, respectively.

Table 2. TD-DFT absorption energies and main compositions of the low-lying electronic transitions for **L¹** and its $Y(tta)_3$ derivative. In addition, the charge transfer and the pure intramolecular transitions are reported. ID, IA, Itta and H, L represent the Intramolecular Donor (TTF), Intramolecular Acceptor (benzothiazole-2-pyridine, bztp), Intramolecular 2-thenoyltrifluoroacetonate anion (tta^-), the HOMO and the LUMO, respectively. Therefore, ILCT stands for Intra-Ligand Charge Transfer. * Experimentally the ILCT and Itta transitions are fused in a single experimental decomposition due to their very close energy positions.

	Energy exp (cm^{-1})	Energy theo (cm^{-1})	Osc.	Type	Assignment	Transition
L¹	22000	18878	0.25	ILCT	$\pi_{TTF}\rightarrow\pi^*_{bztp}$	H→L (98%)
	28200	28148	0.11	ID	$\pi_{TTF}\rightarrow\pi^*_{TTF}$	H→L+1/+2/+3 (32/18/46%)
	29800	29455	1.09	ILCT	$\pi_{TTF}\rightarrow\pi^*_{bztp}$	H-1→L (89%)
	32900	32743 + 33177	0.20 + 0.11	ILCT	$\pi_{TTF}\rightarrow\pi^*_{bztp}$	H-6→L (93%) + H-2→L (57%)
		34060	0.17		$\pi_{TTF}\rightarrow\pi^*_{TTF}$	H→L+6/+8/+9
	38100	+ 35563	0.17	ID		(85/17/17%)
	44500	40532	0.05	ILCT	$\pi_{TTF}\rightarrow\pi^*_{bztp}$	H-7→L (30%)
		44312	0.04			H-10→L (53%)
	20500	16526	0.25	ILCT	$\pi_{TTF}\rightarrow\pi^*_{bztp}$	H→L (99%)
	27600	27640	0.60	ILCT	$\pi_{TTF}\rightarrow\pi^*_{bztp}$	H-3→L (76%)
		31137	0.29	Itta	$\pi_{tta}\rightarrow\pi^*_{tta}$	H-4→L+1 (22%)
	29700*	31909	1.27			H-1→L+3 (39%)
$Y(tta)_3(L^1)$		31625	0.40	ILCT	$\pi_{TTF}\rightarrow\pi^*_{bztp}$	H-5→L (52%)
	32100	33810	0.12	ID	$\pi_{TTF}\rightarrow\pi^*_{TTF}$	H→L+9 (60%)
	37100	35539	0.17	ILCT	$\pi_{TTF}\rightarrow\pi^*_{bztp}$	H→L+8 (62%)
		35662	0.06			H→L+16 (19%)
	44100	/	/	/	/	/

Additional intense absorption excitation has been observed around 29700 cm^{-1} that corresponds to π-π* intra-tta^- excitations.[23] It is worth noticing that experimentally this new intense absorption band includes the HOMO-5→LUMO ILCT excitation. The UV-visible absorption properties of the ligand **L¹** and Y^{III} coordination complex have been also studied in solid-state (Figures S8 and S9). The absorption spectra have been decomposed into seven bands (Table S2). The lowest-energy additional absorption band (15400 cm^{-1} for **L¹** and 15700 cm^{-1} for Y^{III} analogue) which is observed in the solid-state spectra is due to the intermolecular CT.[48]

Emission Properties

Ligand L¹. The solid-state emission spectra of the ligand **L¹** are represented in Figure 9a. At room temperature, excitation at 22500 cm^{-1} (450 nm) in the π-π* HOMO→LUMO ILCT (see absorption properties section) of **L¹** results in a weak broad ligand-centred emission with a maximum at 13850 cm^{-1}. At 77 K, the emission became slightly more structured with two maxima at 14450 cm^{-1} and 13780 cm^{-1}.

Ligand L². No emission for **L²** was detected.

Yb^{III} based-complexes. Attempts to measure the luminescence of compounds **2** and **4** failed because no detectable Yb^{III}-centred luminescence was observed. Replacing the $hfac^-$ ancillary ligand by tta^- switches on the Yb^{III} luminescence. Emission properties of **5** were measured in solid-state at 77 K (Figure 9b). The characteristic luminescence profile of Yb^{III} corresponding to $^2F_{5/2}\rightarrow{}^2F_{7/2}$ transition is observed upon irradiation at 22200 cm^{-1} (450 nm). The absence of any residual ligand-centred emission in the visible region indicates that the energy-transfer process is rather efficient as observed for the Er^{III} analogue. As already observed in previously published TTF-based complexes of Yb^{III}, the antenna-effect sensitization process is favoured compared to direct f-f excitation and proceeds through energy transfer from the singlet CT state of the **L¹** chromophore.[23],[49]-[51]

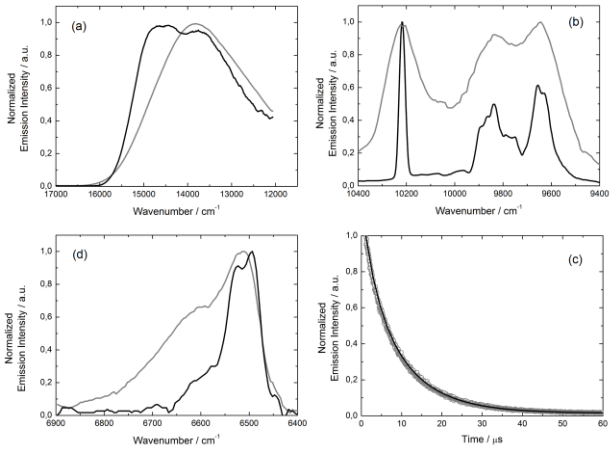

Figure 9. (a) Solid-state emission spectra at room temperature (grey line) and 77 K (black line) of **L¹** in the visible range for λ_{ex}=22500 cm^{-1} (450 nm (b) Solid-state luminescence spectra of **5** at room temperature (grey line) and 77 K (black line) in the NIR range for λ_{ex}=22200 cm^{-1} (450 nm)(corresponding to the main text). Spectra are normalised and not drawn on the same vertical scale. (c) Emission decay of **5** recorded at 10200 cm^{-1} (980 nm) in solid-state at room temperature under 22200 cm^{-1} (450 nm)(corresponding to the main text) excitation. The black line represents the monoexponential fit. (d) Solid-state luminescence spectra of **6** at room temperature (grey line) and 77 K (black line) in the NIR range for λ_{ex}=20000 cm^{-1} (500 nm). Spectra are normalised and not drawn on the same vertical scale.

Eight emission maxima and shoulders are clearly identified at the following energies: 9629 cm^{-1}, 9657 cm^{-1}, 9756 cm^{-1}, 9780 cm^{-1}, 9838 cm^{-1}, 9867 cm^{-1}, 9896 cm^{-1} and 10220 cm^{-1} (Figure 9b). This number of contributions is higher than the degeneracy of the $^2F_{7/2}$ ground-state (Kramers doublets, maximum of 4

contributions). By analogy with our previous works[27],[28],[46],[52] and the one by Auzel *et al.*[53], the additional emission contributions could be attributed to transitions coming from the second or/and third M_J states of the $^2F_{5/2}$ multiplet state and/or vibronic contributions. At this stage, it is difficult to discriminate between both mechanisms. The total splitting is determined equal to 591 cm^{-1}. From the literature, the values of this splitting for an Yb^{III} ion in a distorted and regular D_3 symmetry[54] are 455 cm^{-1} and 372 cm^{-1}, respectively while a splitting of 528 cm^{-1} is found for an Yb^{III} complex[55] in a lower symmetry. The value of 591 cm^{-1} seems thus to correspond to a quite low symmetry that is in agreement with the distortion induced by the two nitrogen and six oxygen atoms as first neighbours of the Yb^{III} ion in **5**. The perfect monoexponential fitting of the luminescence decay plot attests the purity of the sample and corresponds to a lifetime value of 8µs at room temperature (Figure 9c).

Er^{III} based-complex. Emission properties of **6** were measured in solid-state at 77 K and room temperature (Figure 9d). Upon irradiation at 20000 cm^{-1} in the lowest-energy absorption band (π-π* HOMO→LUMO ILCT), one emission band centred at 6494 cm^{-1} (1540 nm) is observed, characteristic of the Er^{III} $^4I_{13/2}\rightarrow{}^4I_{15/2}$ transition. No more residual visible emission of the ligand is observed. This is the signature of an efficient energy transfer to the excited spectroscopic states of the Er^{III} ion. By increasing the temperature, the signal became broader but the shape and energy-position of the maximum remain almost unchanged. It was recently demonstrated that the presence of a low-energy ILCT transition can efficiently sensitized NIR emitters luminescence including Er^{III} ions.[48],[49]

Magnetic Properties

The temperature dependences of $\chi_M T$, with χ_M the molar magnetic susceptibility and T the temperature in Kelvin, for the six compounds is represented on Figure 10. At room temperature all values agree with the calculated $\chi_M T$'s for the multiplet ground states $^6H_{15/2}$ (14.14 cm^3 K mol^{-1}) for Dy^{III}, $^2F_{7/2}$ (2.57 cm^3 K mol^{-1}) for Yb^{III} and $^4I_{15/2}$ (11.48 cm^3 K mol^{-1}) for Er^{III}. $\chi_M T$'s decrease on cooling due to the thermal depopulation of the Stark sublevels. At 2 K, magnetization reaches saturation under 50 kOe for compounds **1**-**5** while for **6** the magnetization linearly increases at high field (Figure S10).

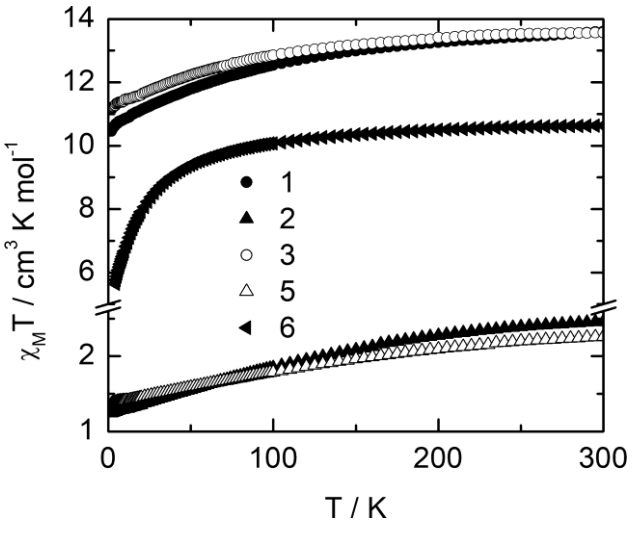

Figure 10. Temperatures dependences of $\chi_M T$ for all compounds. Values are provided for one magnetic centre.

For the compounds **2**, **4**, **5** and **6** there is no slowing of magnetization measured by standard ac measurements on cooling down in the absence of external dc field while it is the case for **1** and **3**. Indeed, both compounds show frequency dependent out-of-phase component of the ac susceptibility at low temperature in zero dc field (Figure 11a and 12a for **1** and **3**, respectively). Careful examination for **1** reveals that two relaxations processes take place. This is characterized by the dissymmetry of the relaxation profile on the χ_M" *vs.* ν curves (Figure 11a) at very low temperatures (T<3 K). This is in line with the presence of two crystallographic sites with two different environments: Dy1 lies in square antiprismatic environment while the coordination polyhedron of Dy2 is halfway between triangular dodecahedron and square antiprism. All attempts to separate the two components were unsuccessful. However, it is perfectly possible to reproduce the experimental data with only one relaxation process in zero field. The relaxation time, τ, is extracted from χ_M" *vs.* ν and χ_M *vs.* ν curves fitted simultaneously with an extended Debye model (see SI, Table S5). As expected the τ distribution, visualised by the empiric parameter α, is relatively large (α~0.3, Table S5) due to the presence of two relaxing sites. The thermal variation of τ can be reproduced with an Arrhenius law slightly modified to account for a temperature independent regime at low temperature: $\tau^{-1}=\tau_0^{-1}\exp(-\Delta/T)+\tau_{TI}^{-1}$. The best fit is obtained with $\tau_0=2.6(8)\times10^{-5}$ s, $\Delta=26$ K and $\tau_{TI}=9.3(5)\times10^{-4}$ s (Figure 13). The application of an external dc field dramatically slows down the relaxation in the temperature regime (Figure 11b). The relaxation time follows also a thermally activated regime in the whole temperature range below 12 K (Table S6) with an Arrhenius evolution only above 7 K ($\tau_0=2.6(1)\times10^{-6}$ s and $\Delta=53$ K).

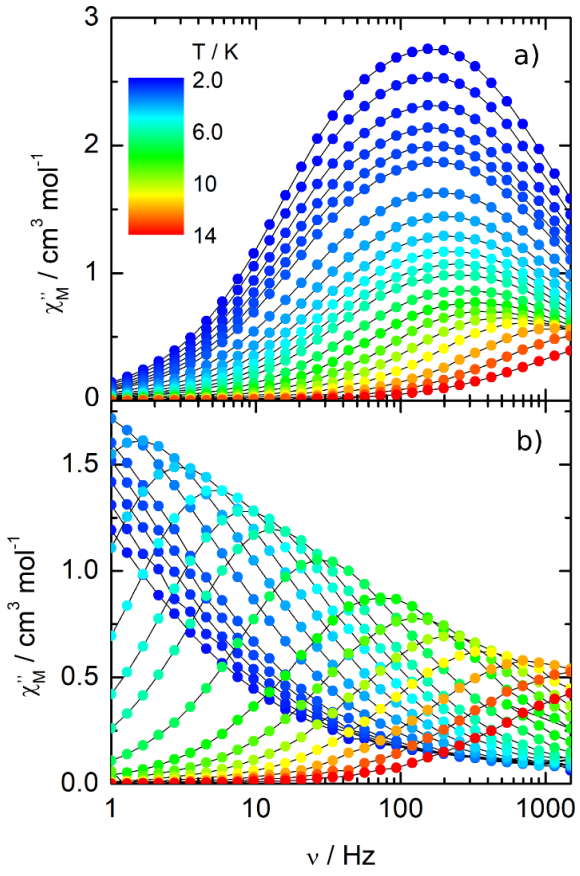

Figure 11. Frequency dependence of the out-of-phase component, χ_M", of the ac susceptibility for **1** in zero field (a) and at 1 kOe (b).

An identical behaviour is observed for **3** in zero field and at 1 kOe (Table S7 and S8) with, in zero field, $\tau_0=3.4(6)\times10^{-5}$ s, $\Delta=19$ K and $\tau_{TI}=3.3(7)\times10^{-4}$ s, and at 1 kOe, $\tau_0=5.9(3)\times10^{-6}$ s, $\Delta=44$ K above 7 K (Figure 13). Globally, **1** and **3** behave similarly except in zero field where the temperature independent regime appears faster for **1** than for **3**.

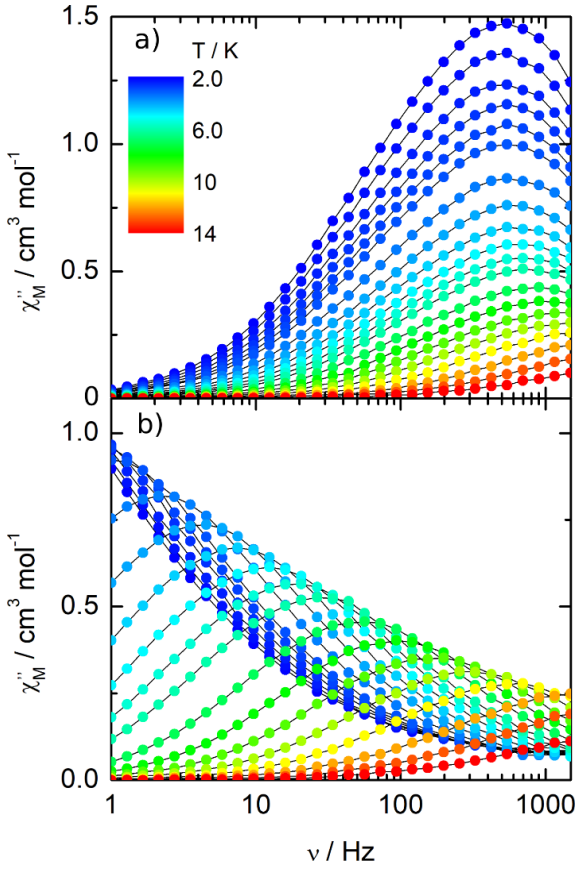

Figure 12. Frequency dependence of the out-of-phase component, χ_M'', of the ac susceptibility for **3** in zero field (a) and at 1 kOe (b).

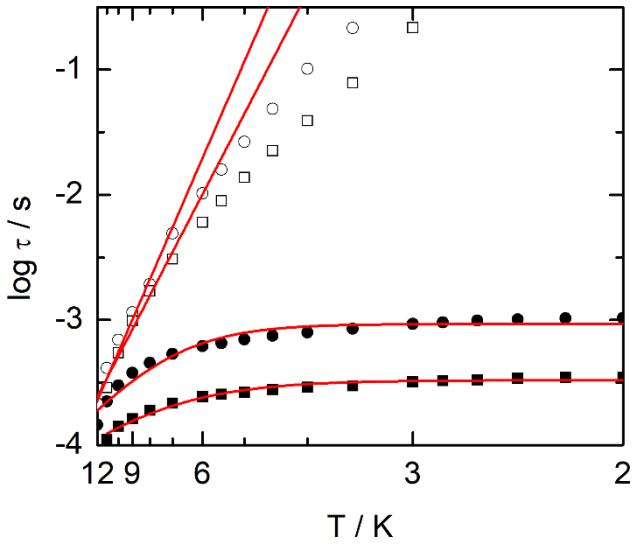

Figure 13. Thermal variations of the relaxation times for compounds **1** (circles) and **3** (squares) at zero field (full symbols) and at 1 kOe (empty symbols). The best fitted curves (see text) are represented in red lines.

Conclusions

Six mononuclear complexes ($[Ln_2(hfac)_6(\mathbf{L^1})_2]\cdot C_6H_{14}\cdot xCH_2Cl_2$ (Ln = Dy and x = 0.25 (**1**); Ln = Yb and x = 0.30 (**2**)), $[Ln(hfac)_3(\mathbf{L^2})]$ (Ln = Dy (**3**), Yb (**4**)) and $[Ln(tta)_3(\mathbf{L^1})]$ (Ln = Yb (**5**), Er (**6**)) ($hfac^-$ = 1,1,1,5,5,5-hexafluoroacetylacetonate; tta^- = 2-thenoyltrifluoroacetylacetonate) have been elaborated using the two redox-active ligands 4-[6-(1,3-benzothiazol-2-yl)pyridin-3-yl]-4',5'-bis(methylthio)tetrathiafulvene ($\mathbf{L^1}$) and 4-[6-(1,3-benzothiazol-2-yl)pyridin-3-yl]-4',5'-(ethylenedithio)tetrathiafulvene ($\mathbf{L^2}$). The X-ray diffraction on single crystals revealed that the lanthanide ion lies in a N2O6 coordination environment.

The Dy^{III} derivatives present an SMM behavior in zero magnetic field. Even if the Dy^{III} ion in **3** adopts a more symmetrical environment, it relaxes faster than in **1** showing that the symmetry could not be the most important parameter in the observation of the slow magnetic relaxation.

The NIR emission wasn't detected for **2** and **4** while the characteristic $^2F_{5/2}\rightarrow{}^2F_{7/2}$ and $^4I_{13/2}\rightarrow{}^4I_{15/2}$ transitions have been observed for **5** and **6**, respectively. Such observation demonstrated the crucial role of the nature of the β-diketonate ligands ($hfac^-$ vs tta^-) in addition to the well-known role of the organic chromophore on the sensitization of the NIR luminescence.

Experimental Section

General Procedures and Materials. The precursors $Ln(hfac)_3\cdot2H_2O$ and $Ln(tta)_3\cdot2H_2O$ (Ln = Er^{III} and Yb^{III}, $hfac^-$ = 1,1,1,5,5,5-hexafluoroacetylacetonate and tta^- = 2-thenoyltrifluoroacetonate anion)[57],[58], 4-[6-(1,3-benzothiazol-2-yl)pyridin-3-yl]-4',5'-bis(methylthio)tetrathiafulvene ($\mathbf{L^1}$),[43] 4,5-(ethylenedithio)tetrathiafulvalene[59] and 2-(5-bromopyridin-2-yl)-1,3-benzothiazole[60],[61] were synthesized following previously reported methods. All other reagents were purchased from Aldrich Co., Ltd. and used without further purification.

Synthesis of 4-[6-(1,3-benzothiazol-2-yl)pyridin-3-yl]-4',5'-(ethylenedithio)tetrathiafulvene ($\mathbf{L^2}$). To a stirred solution of 4,5-(ethylenedithio)tetrathiafulvalene (448 mg, 1.52 mmol) in dry THF (59 mL) at –78°C under N_2 atmosphere was added ^{n}BuLi (1.6 M in hexane, 1.03 mL, 1.66 mmol) and stirring continued for 1 h at –78°C. Tributylstannyl chloride (0.50 mL, 1.66 mmol) was added, the mixture was stirred for a further 1 h at –78°C. The temperature was allowed to rise to room temperature over a period of 5 h, and the solvent was evaporated, water was added (50 mL) and the mixture was extracted with chloroform. The combined organic extracts were washed with water, dried (Na_2SO_4), and the solvent was evaporated in vacuo. Subsequently, dry toluene (63 mL) was added and N_2 gas bubbling was done for 20 min. After the bubbling, 2-(5-bromopyridin-2-yl)-1,3-benzothiazole (305 mg, 1.05 mmol) and $Pd(PPh_3)_2Cl_2$ (370 mg, 0.52 mmol) were added and the mixture was heated overnight at 110°C. The solvent was evaporated. The resulting residue was purified by a column-chromatography on silica gel with CS_2/CH_2Cl_2 (1/1, v/v) as an eluent. Ligand $\mathbf{L^2}$ was afforded as a purple solid (62 mg, 0.11 mmol, 12%); m.p. 255-257°C (decomp.) Rf=0.3 (CS_2/CH_2Cl_2=6/1)

^{1}H NMR (400 MHz, $CDCl_3$): δ 8.74 (d, J=2.0 Hz, 1H, pyridine), 8.37 (d, J=8.5 Hz, 1H, BZT), 8.09 (d, J=8.5 Hz, 1H, BZT), 7.97 (d, J=7.8 Hz, 1H, pyridine), 7.81 (dd, J=7.8 Hz, J=2.0 Hz, 1H, pyridine), 7.52 (dd, J_1=8.5 Hz, J_2=8.5 Hz, 1H, BZT) 7.44 (dd, J_1=8.5 Hz, J_2=8.5 Hz, 1H, BZT), 6.76 (s, 1H, TTF), 3.32 (s, 4H, SCH_2CH_2S)

HRMS (FAB+, Matrix=3-Nitrobenzyl alcohol) ($C_{20}H_{12}N_2S_7$): Found 503.9046; Calcd.503.9028

I.R. (KBr): 757, 982, 1471, 1567, 3056 and 3446 cm^{-1}

Synthesis of complexes

$[Ln_2(hfac)_6(\mathbf{L^1})_2]\cdot C_6H_{14}\cdot xCH_2Cl_2$ (Ln = Dy and x = 0.25 (1); Ln = Yb and x = 0.30 (2)). 0.02 mmol of $Ln(hfac)_3\cdot2H_2O$ (17.3 mg for Ln=Dy and 17.5 mg for Ln=Yb) were dissolved in 10 mL of CH_2Cl_2 and then added to a solution of 10 mL of CH_2Cl_2 containing 10.4 mg of $\mathbf{L^1}$ (0.02 mmol). After 20 minutes of stirring, 30 mL of *n*-hexane were layered at room temperature in the dark. Slow diffusion following by slow evaporation leads to purple single crystals (sticks) which are suitable for X-ray studies. Yield: 16.4 mg (61 %) and 15.5 mg (57 %) respectively for **1** and **2**. Anal. Calcd (%) for $C_{76.25}H_{48.50}Cl_{0.50}F_{36}N_4O_{12}S_{14}Dy_2$: C 34.04, H 1.80, N 2.08; found: C 34.12, H 1.91 N, 2.13. Anal. Calcd (%) for $C_{76.30}H_{48.60}Cl_{0.60}F_{36}N_4O_{12}S_{14}Yb_2$: C 33.74, H 1.79, N 2.06; found: C 33.99, H 1.87 N, 2.16. representative I.R. (KBr): 3144, 3102, 3072, 2960, 2926, 2855, 1651, 1560, 1533, 1506, 1258, 1207, 1144, 802, 762, 662 and 590 cm^{-1}.

$[Ln(hfac)_3(\mathbf{L^2})]$ (Ln = Dy (3) and Yb (4)). 0.02 mmol of $Ln(hfac)_3\cdot2H_2O$ (17.3 mg for Ln=Dy and 17.5 mg for Ln=Yb) were dissolved in 10 mL of CH_2Cl_2 and then added to a solution of 10 mL of CH_2Cl_2 containing 10.4 mg of $\mathbf{L^2}$ (0.02 mmol). After 20 minutes of stirring, 30 mL of *n*-hexane were layered at room temperature in the dark. Slow diffusion following by slow evaporation leads to purple single crystals

(sticks) which are suitable for X-ray studies. Yield: 19.8 mg (77 %) and 21.0 mg (81 %) respectively for **3** and **4**. Anal. Calcd (%) for $C_{35}H_{15}DyF_{18}N_2O_6S_7$: C 32.60, H 1.16, N 2.17; found: C 32.52, H 1.21 N, 2.13. Anal. Calcd (%) for $C_{35}H_{15}YbF_{18}N_2O_6S_7$: C 32.33, H 1.15, N 2.16; found: C 32.41, H 1.17 N, 2.19.Representative I.R. (KBr): 2927, 2851, 1653, 1558, 1533, 1506, 1256, 1211, 1146, 802, 762, 662 and 590 cm^{-1}

[Ln(tta)$_3$(L^1)] (Ln=Er (5) and Yb (6)). 0.02 mmol of Ln(tta)$_3$·2H$_2$O (17.3 mg for Ln=Er and 17.5 mg for Ln=Yb) were dissolved in 10 mL of CH_2Cl_2 and then added to a solution of 10 mL of CH_2Cl_2 containing 10.4 mg of **L^1** (0.02 mmol). After 20 minutes of stirring, 30 mL of *n*-hexane were layered at room temperature in the dark. Slow diffusion following by slow evaporation leads to purple single crystals (sticks) which are suitable for X-ray studies. Yield: 21.9 mg (82 %) and 23.6 mg (88 %) respectively for **5** and **6**. Anal. Calcd (%) for $C_{44}H_{26}F_9N_2O_6S_{10}Er$: C 39.48, H 1.94, N 2.09; found: C 39.52, H 2.01 N, 2.13. Anal. Calcd (%) for $C_{44}H_{26}F_9N_2O_6S_{10}Yb$: C 39.31, H 1.94, N 2.08; found: C 38.99, H 1.67 N, 2.14. Representative I.R. (KBr): 3101, 2955, 2853, 1628, 1541, 1506, 1412, 1358, 1314, 1247, 1231, 1188, 1143, 1063, 1038, 935, 787, 717, 642 and 584 cm^{-1}

Crystallography. Single crystals of **1-6** were mounted on a APEXII Bruker-AXS diffractometer for data collection (MoKα_α radiation source, λ = 0.71073 Å, T = 150(2) K) from the Centre de Diffractométrie (CDIFX), Université de Rennes 1, France. Structures were solved with a direct method using the SHELXT program[62] and refined with a full matrix least-squares method on F^2 using the SHELXL-14/7 program[63]. Crystallographic data are summarized in Table 1. Complete crystal structure results as a CIF file including bond lengths, angles, and atomic coordinates are deposited as Supporting Information.

Physical Measurements. The elementary analyses of the compounds were performed at the Centre Régional de Mesures Physiques de l'Ouest, Rennes. ^{1}H NMR was recorded on a Bruker Ascend 400 spectrometer. Chemical shifts are reported in parts per million referenced to TMS for ^{1}H NMR. Cyclic voltametry was carried out in CH_2Cl_2 solution, containing 0.1 M $N(C_4H_9)_4PF_6$ as supporting electrolyte. Voltamograms were recorded at 100 mV s^{-1} at a platinum disk electrode. The potentials were measured *versus* a saturated calomel electrode (SCE). Absorption spectra were recorded on a Varian Cary 5000 UV-Visible-NIR spectrometer equipped with an integration sphere. The luminescence spectra were measured using a Horiba-Jobin Yvon Fluorolog-3® spectrofluorimeter, equipped with a three slit double grating excitation and emission monochromator with dispersions of 2.1 nm/mm (1200 grooves/mm). The steady-state luminescence was excited by unpolarized light from a 450 W xenon CW lamp and detected at an angle of 90° by a red-sensitive Hamamatsu R928 photomultiplier tube. Spectra were reference corrected for both the excitation source light intensity variation (lamp and grating) and the emission spectral response (detector and grating). Near infra-red spectra were recorded at an angle of 90° using a liquid nitrogen cooled, solid indium/gallium/arsenic detector (850-1600 nm). All solid state measurements were performed in quartz tube. 77K measurement was done using by cooling the sample in a dewar in the sample compartment. 10K measurement was performed in an Oxford instruments® Optistat^{TM} CF2 cryostat cooled down with liquid helium. The excitation of the Yb^{III} luminescence decays was performed with an optical parametric oscillator from EKSPLA NT342, pumped with a pulsed frequency tripled YAG:Nd laser. The pulse duration was 6 ns at 10 Hz repetition rate. The detection was ensured by a R1767 Hamamatsu photomultiplier through a Jobin-Yvon monochromator equipped with a 1 µm blazed grating. The signal was visualized and averaged with a Lecroy digital oscilloscope LT342. The dc magnetic susceptibility measurements were performed on solid polycrystalline sample with a Quantum Design MPMS-XL SQUID magnetometer between 2 and 300 K in an applied magnetic field of 1 kOe in the 2-20 K temperature range and 10 kOe between 20 and 300 K. These measurements were all corrected for the diamagnetic contribution as calculated with Pascal's constants.

Computational Details. DFT geometry optimizations and TD-DFT excitation energy calculations of the ligand **L^1** and its Y^{III} analogue were carried out with the Gaussian 09 (revision A.02) package[64] employing the PBE0 hybrid functional.[65],[66] The "Stuttgart/Dresden" basis sets and effective core potentials were used to describe the yttrium atom,[67] whereas all other atoms were described with the SVP basis sets.[68] The first 50 monoelectronic excitations were calculated. In all steps, a modeling of bulk solvent effects (solvent=dichloromethane) was included through the Polarizable Continuum Model (PCM),[69] using a linear-response non-equilibrium approach for the TD-DFT step.[70],[71] Molecular orbitals were sketched using the Gabedit graphical interface.[72]

Supporting Information (see footnote on the first page of this article): Ortep views for compounds **1-6**, Tables of selected bond lengths and analyses of the coordination polyhedra around Ln in compounds **1-6**, cyclic voltammetry, additional photo-physical and magnetic measurements. Complete crystal structure results as a CIF file including bond lengths, angles, and atomic coordinates are deposited as Supporting Information. CCDC 1558616-1558619, 1510235, 1510238 contain the supplementary crystallographic data for the compounds **1-6** respectively. These data can be obtained free of charge from the Cambridge Crystallographic Data Centre via www.ccdc.cam.ac.uk/data_request/cif)

Acknowledgments

This work was supported by the CNRS, Rennes Métropole, Université de Rennes 1, Région Bretagne, FEDER and Agence Nationale de la Recherche (N° ANR-13-BS07-0022-01). B.L.G. thanks the French GENCI-CINES center for high-performance computing resources. The authors thank Miss Chika Hashimoto for the synthesis of **L^1** ligand.

[1] D. N. Woodruff, R. E. P. Winpenny, R. A. Layfield, *Chem. Rev.* **2013**, *113*, 5110-5148.

[2] H.L.C. Feltham, S. Brooker, *Coord. Chem. Rev*. 2014, 276, 1-33.

[3] P. Zhang, Y.-N. Guo, J. Tang, *Coord. Chem. Rev*. 257 (2013) 1728.

[4] F. Pointillart, O. Cador, B. Le Guennic, L. Ouahab, *Coord. Chem. Rev.* **2017**, *346*, 150-175.

[5] D. Parker, *Chem. Soc. Rev.* **2004**, *33*, 156-165.

[6] J.-C. G. Bünzli, C. Piguet, *Chem. Soc. Rev.* **2005**, *54*, 1048-1077.

[7] S. V. Eliseeva, J.-C. G. Bünzli, *Chem. Soc. Rev*. **2010**, *39*, 189-227.

[8] M. N. Leuenberger, D. Loss, *Nature* **2001**, *410*, 789–793.

[9] P. Santini, S. Carretta, F. Troiani, G. Amoretti, *Phys. Rev. Lett.* **2011**, *107*, 230502.

[10] C. J. Wedge, G. A. Timco, E. T. Spielberg, R. E. George, F. Tuna, S. Rigby, E. J. L. McInnes, R. E. P. Winpenny, S. J. Blundell, A. Ardavan, *Phys. Rev. Lett.* **2012**, *108*, 107204.

[11] S. Hill, R. S. Edwards, N. Aliaga-Alcalde, G. Christou, *Science* **2003**, *302*, 1015–1018.

[12] L. Bogani, W. Wernsdorfer, *Nat. Mater.* **2008**, *7*, 179–186.

[13] S. Thiele, F. Balestro, R. Ballou, S. Klyatskaya, M. Ruben, W. Wernsdorfer, *Science* **2014**, *344*, 1135–1138.

[14] M. Ganzhorn, S. Klyatskaya, M. Ruben, W. Wernsdorfer, *Nat. Nanotechnol.* **2013**, *8*, 165–169.

[15] M. Urdampilleta, S. Klyatskaya, J.-P. Cleuziou, M. Ruben, W. Wernsdorfer, *Nat. Mater.* **2011**, *10*, 502–506.

[16] K. Kuriki, Y. Koike and Y. Okamoto, *Chem. Rev.* **2002**, *102*, 2347–2356.

[17] E. G. Moore, A. P. S. Samuel, K. N. Raymond, *Acc. Chem. Res.* **2009**, *42*, 542–552, and references therein.

[18] J.-C. G. Bünzli, *Chem. Rev.* **2010**, *110*, 2729–2755.

[19] R. M. Duke, E. B. Veale, F. M. Pfeffer, P. E. Kruger, T. Gunnlaugsson, *Chem. Soc. Rev.* **2010**, *39*, 3936–3953.

[20] A. Beeby, S. W. Botchway, I. M. Clarkson, S. Faulkner, A. M. Parker, D. Parker, J. A. G. Williams, *J. Photochem. Photobiol., B*, **2000**, *57*, 83–89.

[21] A. Grichine, A. Haefele, S. Pascal, A. Duperray, R. Michel, C. Andraud, O. Maury, *Chem. Sci.* **2014**, *5*, 3475–3485.

[22] G. Cucinotta, M. Perfetti, J. Luzon, M. Etienne, P. E. Car, A. Caneschi, G. Calvez, K. Bernot, R. Sessoli, *Angew. Chem., Int. Ed.* **2012**, *51*, 1606−1610.

[23] F. Pointillart, B. Le Guennic, S. Golhen, O. Cador, O. Maury, L. Ouahab, *Chem. Commun*. **2013**, *49*, 615−617.

[24] J. Long, R. Vallat, R. A. S. Ferreira, L. D. Carlos, F. A. A. Paz, Y. Guari, J. Larionova, *Chem. Commun*. **2012**, *48*, 9974-9976.

[25] K. Yamashita, R. Miyazaki, Y. Kataoka, T. Nakanishi, Y. Hasegawa, M. Nakano, T. Yamamura, T. Kajiwara, *Dalton Trans.* **2013**, *42*, 1987-1990.

[26] K. Ehama, Y. Ohmichi, S. Sakamoto, T. Fujinami, N. Matsumoto, N. Mochida, T. Ishida, Y. Sunatsuki, M. Tsuchimoto, N. Re, *Inorg. Chem.* **2013**, *52*, 12828-12841.

[27] M. Ren, S.-S. Bao, R. A. S. Ferreira, L.-M. Zheng, L. D. Carlos, *Chem. Commun.* **2014**, *50*, 7621-7624.

[28] X. Yi, K. Bernot, V. Le Corre, G. Calvez, F. Pointillart, O. Cador, B. Le Guennic, J. Jung, O. Maury, V. Placide, Y. Guyot, T. Roisnel, C. Daiguebonne, O. Guillou, *Chem. Eur. J.* **2014**, *20*, 1569-1576.

[29] K. Soussi, J. Jung, F. Pointillart, B. Le Guennic, B. Lefeuvre, S. Golhen, O. Cador, Y. Guyot, O. Maury, L. Ouahab *Inorg. Chem. Front.* **2015**, *2*, 1105-1117

[30] F. Pointillart, B. Le Guennic, O. Cador, O. Maury, L. Ouahab, *Acc. Chem. Res.* **2015**, *48*, 2834-2842.

[31] J. Ferraris, D. O. Cowan, V. Walatka, J. H. Perlstein, *J. Am. Chem. Soc.* **1973**, *95*, 948-949.

[32] F. Pointillart, S. Golhen, O. Cador, L. Ouahab, *Dalton Trans.*, **2013**, *42*, 1946-1960 and references therein.

[33] L. Hu, W. Liu, C.-H. Li, X.-H. Zhou, J.-L. Zuo, *Eur. J. Inorg. Chem.* **2013**, 6037-6048.

[34] X. Xiao, W. Pan, Z. Wang, Z. Shen, L. Shen, J. Fang, H. Gao, X. Li, H. Fujiwara, *Synthetic Metals* **2014**, 189, 42-46.

[35] F. Pointillart, S. Golhen, O. Cador, L. Ouahab, *C. R. Chimie* **2013**, 16, 679-688.

[36] H. Douib, F. Pointillart, B. Lefeuvre, B. Golhen, S. Golhen, O. Cador, B. Le Guennic, A. Gouasmia, L. Ouahab, *Eur. J. Inorg. Chem.* **2016**, 5630-5639.

[37] F. Pointillart, Y. Le Gal, S. Golhen, O. Cador, L. Ouahab, *Inorg. Chem.* **2008**, *47*, 9730-9732.

[38] H. Cui, T. Otsuka, A. Kobayashi, N. Takeda, M. Ishikawa, Y. Misaki, H. Kobayashi, *Inorg. Chem.* **2003**, *42*, 6114-6122 and references therein.

[39] H. Tanaka, H. Kobayashi, A. Kobayashi P. Cassoux, *Adv. Mater.* **2000**, *12*, 1685-1689.

[40] S.Uji, H. Shinagawa, T. Terashima, C. Terakura, T. Yakabe, Y. Terai, M. Tokumoto, A. Kobayashi, H. Tanaka, H. Kobayashi, *Nature* **2001**, *410*, 908-910.

[41] H. Fujiwara, S. Yokota, S. Hayashi, S. Takemoto, H. Matsuzaka, *Physica B* **2010**, *405*, S15−S18.

[42] S. Yokota, K. Tsujimoto, S. Hayashi, F. Pointillart, L. Ouahab, H. Fujiwara, *Inorg. Chem.* **2013**, *52*, 6543-6550.

[43] Y. Kishi, F. Pointillart, B. Lefeuvre, F. Riobé, B. Le Guennic, S. Golhen,O. Cador, O. Maury, H. Fujiwara, L. Ouahab, *Chem. Commun.* **2017**, *53*, 3575-3578.

[44] M. Llunell, D. Casanova, J. Cirera, J. M. Bofill, P. Alemany, S. Alvarez, S. SHAPE (version 2.1), Barcelona, 2013.

[45] F. Pointillart, B. Le Guennic, T. Cauchy, S. Golhen, O. Cador, O. Maury, L. Ouahab, *Inorg. Chem.* **2013**, *52*, 5978-5990.

[46] J. Jung, T. da Cunha, B. Le Guennic, F. Pointillart, L. M. Pereira, J. Luzon, S. Golhen, O. Cador, O. Maury, L. Ouahab, *Eur. J. Inorg. Chem.* **2014**, 3888−3894.

[47] G. Cosquer, F. Pointillart, B. Le Guennic, Y. Le Gal, S. Golhen, O. Cador, L. Ouahab, *Inorg. Chem.* **2012**, *51*, 8488-8501.

[48] F. Pointillart, T. Cauchy, O. Maury, Y. Le Gal, S. Golhen, O. Cador, L. Ouahab, *Chem.-Eur. J.* **2010**, *16*, 11926-11941.

[49] F. Pointillart, A. Bourdolle, T. Cauchy, O. Maury, Y. Le Gal, S. Golhen, O. Cador, L. Ouahab, *Inorg. Chem.* **2012**, *51*, 978-984.

[50] A. D'Aléo, F. Pointillart, L. Ouahab, C. Andraud, O. Maury, *Coord. Chem. Rev.*, **2012**, *256*, 1604-1620.

[51] D. Aravena, E. Ruiz, *Inorg. Chem.* **2013**, *52*, 13770–13778.

[52] G. Cosquer, F. Pointillart, J. Jung, B. Le Guennic, S. Golhen, O. Cador, Y. Guyot, A. Brenier, O. Maury, L. Ouahab, *Eur. J. Inorg. Chem.* **2014**, 69-82.

[53] P. Goldner, F. Pell, D. Meichenin, F. Auzel, *J. Lumin.* **1997**, *71*, 137–150.

[54] F. R. Gonçalves Silva, O. L. Malta, C. Reinhard, H. U. Güdel, C. Piguet, J. Moser, J.-C. G. Bünzli, *J. Phys. Chem. A* **2002**, *106*, 1670-1677.

[55] G. Lapadula, A. Bourdolle, F. Allouche, M. Conley, I. del Rosa, L. Maron, W. W. Lukens, Y. Guyot, C. Andraud, S. Brasselet, C. Copéret, O. Maury, R. A. Andersen, *Chem. Mater.* **2014**, *26*, 1062−1073.

[56] A. Bourdolle, M. Allali, A. D'Aléo, P. L. Baldeck, K. Kamada, J. A. G. Williams, H. Le Bozec, C. Andraud, O. Maury, *Chem. Phys. Chem.* **2013**, *14*, 3361-3367.

[57] A. I. Vooshin, N. M. Shavaleev, V. P. Kazakov, *J. Luminescence* **2000**, *91*, 49-58.

[58] M. F. Richarsdson, W. F. Wagner, D. E. Sands, *J. Inorg. Nucl. Chem.* **1968**, *30*, 1275-1289.

[59] R. D. McCullough, M. A. Petruska, J. A.; Belot, *Tetrahedron* **1999**, *55*, 9979-9998.

[60] X. Wang, P. Rabbat, P. O'Shea, R. Tillyer, E. J. J. Grabowski, P. J. Reider, *Tetrahedron. Lett.* **2000**, *41*, 4335-4338.

[61] X. Chen, F. J. Femia, J. W. Babich, J. Zubiet, Inorg. Chim. Acta 2001, 314, 91-96.

[62] G. L. Sheldrick, *Acta Crystallogr., Sect. A* **2015,** *71*, 3−8.

[63] G. M. Sheldrick, *Acta Crystallogr. Sect. C* **2015**, *71*, 3-8.

[64] M. J. Frisch, G. W. Trucks, H. B. Schlegel, G. E. Scuseria, M. A. Robb, J. R. Cheeseman, G. Scalmani, V. Barone, B. Mennucci, G. A. Petersson, H. Nakatsuji, M. Caricato, X. Li, H. P. Hratchian, A. F. Izmaylov, J. Bloino, G. Zheng, J. L. Sonnenberg, M. Hada, M. Ehara, K. Toyota, R. Fukuda, J. Hasegawa, M. Ishida, T. Nakajima Y. Honda, O. Kitao, H. Nakai, T. Vreven, Jr. J. A. Montgomery, J. E. Peralta, F. Ogliaro, M. Bearpark, J. J. Heyd, E. Brothers, K. N. Kudin, V. N. Staroverov, R. Kobayashi, J. Normand, K. Raghavachari, A. Rendell, J. C. Burant, S. S. Iyengar, J. Tomasi, M. Cossi, N. Rega, J. M. Millam, M. Klene, J. E. Knox, J. B. Cross, V. Bakken, C. Adamo, J. Jaramillo, R. Gomperts, R. E. Stratmann, O. Yazyev, A. J. Austin, R. Cammi, C. Pomelli, J. W. Ochterski, R. L. Martin, K. Morokuma, V. G. Zakrzewski, G. A. Voth, P. Salvador, J. J. Dannenberg, S. Dapprich, A. D. Daniels, O. Farkas, J. B. Foresman, J. V. Ortiz, J. Cioslowski and D. J. Fox, Gaussian 09 Revision A.02, Gaussian Inc., Wallingford CT, 2009.

[65] J. P. Perdew, K. Burke, M. Ernzerhof, *Phys. Rev. Lett.* **1996**, *77*, 3865-3868.

[66] C. Adamo, V. Barone, *J. Chem. Phys.* **1999**, *110*, 6158-6170.

[67] M. Dolg, H. Stoll, H.-A. Preuss, *Theor. Chim. Acta* **1993**, *85*, 441–450.

[68] F. Weigend, R. Ahlrichs, *Phys. Chem. Chem. Phys.* **2005**, *7*, 3297-3305.

[69] J. Tomasi, B. Mennucci, R. Cammi, *Chem. Rev.* **2005**, *105*, 2999-3093.

[70] M. Cossi, V. Barone, *J. Chem. Phys.* **2001**, *115*, 4708-4717.

[71] R. Improta, V. Barone, G. Scalmani, M. J. Frisch, *J. Chem. Phys.* **2006**, *125*, 054103-054109.

[72] A.-R. Allouche, *J. Comput. Chem.* **2011**, *32*, 174-182.

Entry for the Table of Contents

Layout 1:

Tetrathiafulvalene Complexes

The effect of the nature of the tetrathiafulvalene-based ligand as well as the nature of the ancillary ligand on the luminescence and single-molecule magnet behaviour has been studied for a series of mononuclear complexes of lanthanide ions.

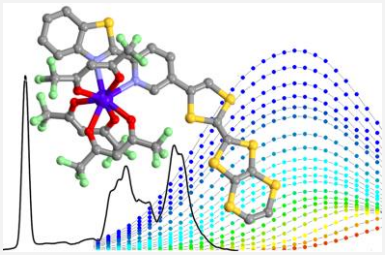

Y. Kishi, L. Cornet, F. Pointillart,* F. Riobé, B. Lefeuvre, O. Cador, B. Le Guennic, O. Maury, H. Fujiwara,* L. Ouahab Page No. – Page No.

Luminescence and Single-Molecule Magnet Behaviour in Lanthanide Coordination Complexes Involving Benzothiazole-Based Tetrathiafulvalene Ligands

Keywords: Tetrathiafulvalene, Lanthanides, Coordination Chemistry, Luminescence, Single-Molecule Magnet